中國機械工程學刊第四十一卷第三期第 265~274 頁(民國一百零九年)
Journal of the Chinese Society of Mechanical Engineers, Vol.41, No.3, pp 265~274 (2020)

Effect of Diffuser Flow on the Performance of Water-Gas Shift Membrane Reactors

Yu-Shao Lin*, Yen-Cho Chen** and Wen-Jenn Sheu*

Keywords : Water-gas shift membrane reactor, Diffuser flow, CO conversion, H_2 recovery

ABSTRACT

The Pd-based water-gas shift membrane reactor (WGS-MR) is a promising technology for pre-combustion CO_2 capture and hydrogen production. A conceptual study on a tubular WGS-MR performance with an inner permeation diffuser flow for the syngas is investigated by numerical simulation. The results reveal that both the CO conversion and H_2 recovery of membrane reactors are improved. From a physical point of view, the time both for WGS reaction and for H_2 permeation through membrane becomes longer as the syngas goes through the channel of diffuser flows. This fact implies that the performance of WGS-MR will be enhanced if the diffuser flow channel is adopted.

INTRODUCTION

Merkel et al. (2012) and Schiebahn et al. (2012) presented integrated gasification combined-cycle (IGCC) with CO_2 capture and sequestration (CCS) is a promising technology for clean energy in the power plants with zero CO_2 emission by using coal, biomass, or municipal waste as feed-stock. For pre-combustion CO_2 capture, the syngas produced from coal gasifier goes through the following processes: particulate removal, gas cleanup for the sulfur removal, the water-gas shift reactor to convert CO and steam to CO_2 and H_2, and a gas separator to separate CO_2 and H_2. The captured CO_2 is further CO_2 sequestration, while the purified H_2 can be used as fuel in the combined cycle of power plant, or in the full cell, or for the various chemical products. The major issue faced by IGCC with CCS is the high cost.

Schiebahn et al. (2012) and Dolan et al. (2010) pointed out that the WGS-MR can reduce cost and increase efficiency. In a WGS-MR, H_2 is removed continuously from the reaction side through membrane such that the higher CO conversion can be obtained according to Le Chatelier’s principle. However, although there are many advantages on the WGS-MR, it still faces several challenges such as expensive Pd membrane, membrane stability, and membrane poisoned by H_2S.

The 1-D model was used by Brunetti et al. (2007), Piemonte et al. (2010) and Gosiewski and Tanczyk (2011) for the WGS-MR performance, since it provides quick preliminary performance values for the reactor design. Boon et al. (2011) indicated that only 2-D model can adequately describe the mass transfer resistances for high transmembrane flux.

In the 2-D modeling, the concentration polarization for H_2 permeation in a Pd-based membrane tube was simulated by Chen et al. (2012). It is concluded that the H_2 permeation rate can be predicted by the Sieverts’ law if the H_2 permeation ratio is not larger than 30%. The hydrogen production from the WGS reaction in a Pd membrane tube was studied by Chen and Lu (2012). The hydrogen production from coal-derived syngas was further investigated by Chen and Chein (2018). Chen et al. (2013) analyzed the influences of geometry and flow pattern on concentration polarization for hydrogen permeation. Marin et al. (2012) found that the space velocity and pressure are the most important parameters affecting membrane reactor performance. The high-temperature WGS-MR was simulated by Chen et al. (2017). Their results revealed that the WGSR proceeds from kinetically controlled reaction to thermodynamically governed one as the temperature of feed gas increases.

Chein et al. (2013) studied numerically the permeance variation effects on performance of WGS-MR by using the pre-exponential factor, Q_0, to account for the membrane permeance. It was shown that three distinct CO conversion regimes exist based on the Q_0 value. For low Q_0, the CO conversion approaches to that of a conventional reactor. For a high Q_0, high CO conversion and H_2 recovery are obtained. For the intermediate Q_0 range both CO conversion and H_2 recovery vary linearly with the Q_0.

Paper Received October, 2018. Revised December,2018. Accepted January, 2019. Author for Correspondence: Wen-Jenn Sheu.

**Department of Power Mechanical Engineering, National Tsing Hua University, Hsinchu, 30013, Taiwan, R.O.C.*

***Department of Energy Engineering, National United University, Miaoli, 36063, Taiwan, R.O.C.*

**corresponding author: Tel: +886-3-5162099; E-mail: wjsheu@mx.nthu.edu.tw*

In the 3-D modeling of the Pd-Ag membrane module for H_2 purification by Coroneo et al. (2009), they found that the H_2 permeation calculations depend on the local determination of the mass transfer resistances offered by the gas phase and by the membrane.

The experimental works in WGS-MR performance at temperature range of 250-400°C were reported by Basile et al. (1996), Barbieri et al. (2008), and Augustine et al. (2012). As indicated in Fig. 2 of Diniz da Costa et al. (2009) and in Fig. 1 of Galuszka et al. (2012), a high temperature WGS-MR incorporared with the hot gas cleaning for particulate and sulfur removals will allow further simplification of the procecess, reduce the cost, and increase the efficiency. Augustine et al. (2011) conducted experiments in a WGS-MR with a simulated syngas feed at 14.0 bar and 400-450°C, a maximum CO conversion of 98.2% was achieved with a H_2 recovery of 81.2% at 450°C.

A Pt/La_2O_3·SiO2 catalyst for the WGS reaction in a Pd-Ag membrane reactor was tested in the range of 400-450°C by Cornaglia et al. (2013). Under the best operating conditions, a CO conversion of 98% and a hydrogen recovery of 90% were reached. Iyoha et al. (2007) demonstrated that Pd and Pd-Cu may be viable membrane materials at a very high temperature of 900°C and 19 atm. However, the water-gas shift environment caused pinhole formation in the membrane surfaces after about 8 days of operation.

From the literature for the tubular WGS-MR, it is found that the syngas and sweeping gas always flow through the straight channels, that is, the diameters of flow channels don't change through the flow direction. The conceptual study for the tubular WGS-MR with a diffuser permeation channel for syngas flow is performed numerically in this work. Physically, the diffuser permeation channel acts to slow down the syngas flow and provides a longer time for water-gas shift reaction and for H_2 permeation through membrane.

FORMULATION

The schematic diagram of a tubular WGS-MR with an inner diffuser flow channel for syngas is shown in Fig. 1. It is composed of two concentric tubes. The inner tube is the reaction channel with an inlet radius of $R_{r,in}$ and an outlet radius of $R_{r,out}$. The reaction side is filled with iron-chrome oxide catalyst pellet with diameter d_{cat}. The syngas flows into the reaction channel. The outer tube is a straight channel with a fixed radius of R_p. The space between the inner and outer tubes is regarded as the permeation side. The Pd-based membrane is located between the reaction side and the permeation side. Nitrogen is used as the sweeping gas for carrying out the H_2, which permeates from the reaction side through the membrane.

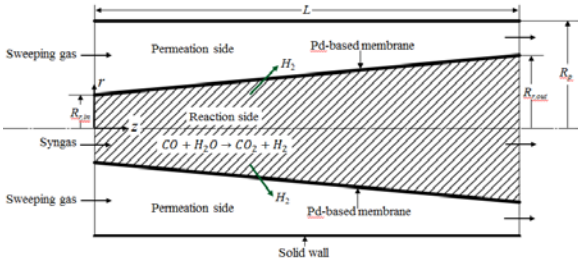

Fig. 1 The schematic of a tubular water-gas shift membrane reactor.

Mathematical Model

The assumptions in this work are as follows.

(1) All component gases are treated as ideal gases.

(2) Flow field can be regarded as an axis-symmetric, laminar and steady flow.

(3) The packed-bed catalyst is treated as a homogeneous porous medium with porosity ε and permeability K. The catalyst is in thermal equilibrium with the surrounding gas.

(4) The membrane has infinite selectivity to the hydrogen and zero selectivity for the other gas species.

(5) Since the membrane is very thin as compared with the reactor size, the membrane is neglected in the computation domain. However, its thickness is taken into account in the hydrogen permeation flux by using the Sieverts' law modeling.

The governing equations of continuity, momentum, energy, and species can be written as below.

$$\nabla \cdot \left(\varepsilon \rho_g \vec{V}\right) = 0 \tag{1}$$

$$\frac{1}{\varepsilon^2}\nabla \cdot (\rho_g \vec{V}\vec{V}) = \nabla \cdot \left[- p\vec{I} + \frac{\mu_g}{\varepsilon}\left(\nabla\vec{V} + (\nabla\vec{V})^T - \frac{2\mu_g}{3\varepsilon}\vec{I}\nabla \cdot \vec{V} \right)\right] + S_u \tag{2}$$

$$\nabla \cdot (\varepsilon \rho_g c_p \vec{V} T) = \nabla \cdot (\lambda_e \nabla T) + q_c \tag{3}$$

$$\nabla \cdot \left\{ \rho_g \vec{V} m_i - \rho_g m_i \sum_{j=1}^{N_G} \left[D_{ij,e}\left(\nabla x_i - (x_i - m_i)\frac{\nabla p}{p} \right) - D_i^T \frac{\nabla p}{p} \right] \right\} = r_i \tag{4}$$

Eq. (2) is known as the Darcy-Brinkman equation, where $\vec{V}$ is the flow velocity vector, p is the pressure, μ_g is the gas mixture viscosity, and ρ_g is the mass-weighted gas mixture density defined as,

$$\rho_g = \frac{p}{R_g T}\sum_{i=1}^{N_G} x_i M_i \tag{5}$$

where N_G is the number of gas species, x_i and M_i are the species molar fraction and molecular weight, respectively. T is the temperature. In Eq. (2), the source term S_u, permeability K_{pe}, and Forchheimer drag coefficient C_f for a packed bed with spherical particles are given by Nield and Bejan (2006)

$$S_u = -\frac{\mu_g}{K}\vec{V} + \frac{\rho_g C_f}{\sqrt{K}}\left|\vec{V}\right|\vec{V}_c, \quad K = \frac{d_{cat}^2 \varepsilon^3}{150(1-\varepsilon)^2},$$

$$C_f = \frac{1.75}{\sqrt{150}\varepsilon^{1.5}} \tag{6}$$

The values of c_p and λ_e in Eq. (3)are given by

$$c_p = \sum_{i=1}^{N_G} m_i c_{p,i}, \ \ \lambda_e = \varepsilon\lambda_g + (1-\varepsilon)\lambda_{cat} \tag{7}$$

where m_i and $c_{p,i}$ are the mass fraction and specific heat, respectively, and λ_e is the effective thermal conductivity coefficient which is composed by gas mixture and catalyst. Eq. (4) is also called Maxwell-Stefan equation from Mills (2001), where r_i, $D_{ij,e}$ and D_i^T are the production rate due to chemical reaction, effective binary gas diffusivity and thermal diffusion coefficient of the i^{th} species, respectively. $D_{ij,e}$ is expressed as

$$D_{ij,e} = D_{ij}\,\varepsilon/\tau \tag{8}$$

where D_{ij} and τ are the binary gas diffusivity in free space and tortuosity of the catalyst pellet, respectively.

Chemical Reaction Model

The water-gas shift reaction is expressed as,

$$CO + H_2O \rightleftharpoons CO_2 + H_2,\ \Delta H_{298K} = -41 \text{ kJ/mol} \tag{9}$$

The reaction rate of water-gas shift reaction under high pressure and temperature using iron-chrome oxide catalyst can be written as by Adams et al (2009),

$$r_{wgs} = \rho_{cat}(1-\varepsilon)F_{press}(1.69\times10^6 \frac{mol}{kg\cdot hr})\exp(-\frac{88000}{R_g T})$$
$$\times x_{CO}^{0.9} x_{H2O}^{0.31} x_{H2}^{-0.05} x_{CO2}^{-0.156}\left(1-\frac{x_{CO2}x_{H2}}{x_{CO}x_{H2O}K_{eq}}\right) \tag{10}$$

where the pressure scale up factor F_{press} by Adams and Barton (2009) and the equilibrium constant K_{eq} by Moe (1962) are defined as,

$$F_{press} = p_{r.}^{0.5-p_r/250},\ \ K_{eq} = \exp(4577.8T - 4.33) \tag{11}$$

Based on Eq. (11), the production rate of each species on the reaction side can be expressed as,

$$r_{CO} = -r_{wgs}M_{CO},\ \ r_{H2O} = -r_{wgs}M_{H2O},$$
$$r_{H2} = r_{wgs}M_{H2},\ \ r_{CO2} = r_{wgs}M_{CO2} \tag{12}$$

The heat source of reaction q_c in Eq. (3) can be expressed as,

$$q_c = -r_{wgs}\Delta H_{wgs} \tag{13}$$

where ΔH_{wgs} is the reaction heat, and it can be expressed as by Vadlamudi and Palanki (2011),

$$\Delta H_{wgs} = -4.912\times10^4 + (c_{p,CO2}M_{CO2} + c_{p,H2}M_{H2}$$
$$-c_{p,CO}M_{CO} - c_{p,H2O}M_{H2O})(T - 298\text{K})\ \text{[J/mol]} \tag{14}$$

Permeation Model

Based on the Sieverts' law from Ward and Dao (1999), the H_2 permeation flux through Pd-based membrane, J_{H_2}, can be physically defined as Eq. (15):

$$J_{H_2} = \frac{Q_0}{\delta}\exp(-\frac{E_m}{R_g T_m})(p_{r,H2}^{1/2} - p_{p,H2}^{1/2}) = K_p(p_{r,H2}^{1/2} - p_{p,H2}^{1/2}) \tag{15}$$

where the unit of J_{H_2} is mol $m^{-2}s^{-1}$, Q_0 is pre-exponential factor with unit mol m^{-1} s^{-1} $Pa^{-0.5}$, δ is the membrane thickness, E_m is the apparent membrane activation energy, T_m is the membrane temperature which is taken as the gas temperature at the membrane in the reaction side, $p_{r,H2}$ and $p_{p,H2}$ are the partial pressures of hydrogen in the reaction and permeate sides, respectively. $K_p = Q_0\exp(-E_m/R_g T_m)/\delta$ is the membrane permeance. Physically, the pre-exponential factor Q_0 is a parameter that represents the performance of membrane fabrication. The value of Q_0 is determined empirically.

Boundary Conditions

The physical domain is divided into two sub-domains: the reaction and permeation sides, as shown in Fig. 1. The boundary conditions of each sub-domain are specified as follows:

(1) At $r = 0$,

$$\frac{\partial\vec{V}}{\partial r} = \frac{\partial T}{\partial r} = \frac{\partial m_i}{\partial r} = 0 \tag{16}$$

where the axi-symmetric conditions are specified along the reaction side center.

(2) At reaction side inlet of $z = 0$

$$\dot{n}_{CO} = \dot{n}_{CO,in},\ \dot{n}_{H2O} = \phi\dot{n}_{CO,in},\ \dot{n}_{H2} = \dot{n}_{CO2} = 0,$$
$$T = T_{r,in},\ u = 0,\ v = 2\bar{v}_{r,in}\left(1 - \left(r/R_{r,in}\right)^2\right) \tag{17}$$

where ϕ is the H_2O/CO molar ratio, $\bar{v}_{r,in}$ is the average velocity in the reaction side. The inlet velocity profile is assumed to be fully developed.

(3) At permeation side inlet of $z = 0$

$$\dot{n}_{N2} = \dot{n}_{N2,in},\ \dot{n}_{H2} = 0,\ T = T_{p,in},\ u = 0\,,$$
$$v = 2\bar{v}_{p,in}\frac{R_p^2 - r^2 + (R_p^2 - R_{r,in}^2)\frac{ln(R_p/r)}{ln(R_{r,in}/R_p)}}{R_p^2 + R_{r,in}^2 - \frac{R_p^2 - R_{r,in}^2}{ln(R_p/R_{r,in})}} \tag{18}$$

where $\bar{v}_{p,in}$ is the average velocity in the permeation side and the fully developed velocity is specified. Nitrogen is used as the sweeping gas.

(4) At reaction side outlet $z = L$

$$p = p_r,\ \ \frac{\partial\vec{V}}{\partial z} = \frac{\partial T}{\partial z} = \frac{\partial m_i}{\partial z} = 0 \tag{19}$$

(5) At permeation side outlet $z = L$

$$p = p_p, \quad \frac{\partial T}{\partial z} = \frac{\partial m_i}{\partial z} = 0 \tag{20}$$

(6) At outer solid wall of reactor for $r = R_p$

$$\vec{V} = \frac{\partial T}{\partial r} = \frac{\partial m_i}{\partial r} = 0 \tag{21}$$

where the no-slip condition and thermal insulation are assumed.

(7) At membrane in reaction side

$$-D_{H2}\frac{\partial(\rho_g m_{H2})}{\partial r} = J_{H2}M_{H2}, \quad \frac{\partial m_{CO}}{\partial r} = \frac{\partial m_{H2O}}{\partial r} = \frac{\partial m_{CO2}}{\partial r} = 0$$

$$V_\perp = \frac{J_{H2}M_{H2}}{\rho_g}, -\lambda_e\frac{\partial T}{\partial r} = (J_{H2}M_{H2}c_{p,H2} + h_m)(T_r - T_p) \tag{22}$$

where $V_\perp$ is the velocity at the direction normal the membrane. As suggested by Madia et al (1999), the heat transfer through membrane can be modeled as a product of the heat transfer coefficient, h_m, at the membrane and temperature difference between the reaction and the permeation sides. In addition, the permeated hydrogen flux also produces a heat flux to the permeation side.

(8) At membrane on permeation side

$$-D_{H2}\frac{\partial(\rho_g m_{H2})}{\partial r} = -J_{H2}M_{H2}, \quad \frac{\partial m_{N2}}{\partial r} = 0, \; V_\perp = -\frac{J_{H2}M_{H2}}{\rho_g}$$

$$, -\lambda_e\frac{\partial T}{\partial r} = -(J_{H2}M_{H2}c_{p,H2} + h_m)(T_r - T_p) \tag{23}$$

The Reynolds numbers both in the reaction and permeation side are between 1 and 30 under all operating conditions in this study. Therefore, laminar flow is assumed.

Numerical Method

All the governing equations with the boundary conditions are solved by COMSOL Multiphysics (COMSOL Inc., version 3.5a). The accuracy of numerical solution depends on the mesh size, and the meshes on boundaries should be finer than those in the central calculation domain. The numerical results show that the mesh-independent results are achieved for the number of elements above 10,000 with a maximum relative variation of 10^{-4}. The mesh number around 60,000 is used to ensure solution accuracy in this study.

The performance of a WGS-MR is evaluated by the CO conversion and H_2 recovery, defined as follows:

$$X_{CO} = (1 - \frac{\dot{n}_{CO,out}}{\dot{n}_{CO,in}}) \times 100\% \tag{24}$$

$$H_2 \text{ recovery} = \frac{\dot{n}_{p,H2,out}}{\dot{n}_{r,H2,out} + \dot{n}_{p,H2,out}} \times 100\% \tag{25}$$

where $\dot{n}_{CO,in}$ and $\dot{n}_{CO,out}$ are the CO molar flow rate at inlet and outlet for the reaction side, respectively. $\dot{n}_{r,H2,out}$ and $\dot{n}_{p,H2,out}$ are the H_2 molar flow rates at the reaction and permeation side outlets, respectively.

Comparison with Experimental Data

The experimental data on the Pd-based water-gas shift membrane reactor provided by Augustine et al (2012) are used for the comparison with the results of numerical model. Their membrane reactor was composed of the 6 cm long (1.3 cm OD) supported Pd-membrane mounted in the center of a 25 cm long (2.1 cm ID) stainless steel tube. The volume of the annular space was 12.8 cm^3 and this space around the membrane was packed with 14.0 g of 48~60 mesh iron-chrome based catalyst (Alfa Aesar, HiFUEL W210). The catalyst bulk density is 1.213 kg/liter given from Alfa Aesar. The CO and steam feed at pressure of 14.4 bar, and the hydrogen permeation side pressure is at 1 bar. The membrane AA-5 was employed for the WGS experiments with a H_2O/CO ratio of 1.1, and its membrane permeance, K_P, was measured as 22.1 $m^3/m^2h\text{-}atm^{0.5}$ at temperature of 450 °C. The membrane AA-6R was used for H_2O/CO ratios of 1.6 and 2.6, and their K_P's at 350 °C, 400 °C, 450 °C, and 500 °C were measured to be 26.9, 31.5, 36.7, and 39.9 $m^3/m^2h\text{-}atm^{0.5}$, respectively.

With the above parameters and operating conditions used as the input data for the present numerical model, the variation of CO conversion (X_{CO}) and H_2 recovery with temperature for H_2O/CO ratio = 1.6 is plotted in Fig. 2(a) for both numerical results and experimental data from Augustine et al. (2012). It is seen that both the tendencies and the quantities of X_{CO}'s and H_2 recovery of numerical results are well consistent with those of the experimental data. The comparison of numerical model with experimental data for the different H_2O/CO ratios at temperature of 450 °C is shown in Fig. 2(b). The model results for H_2O/CO = 1.6 and 2.6 agree well with the experimental data of the membrane AA-6R.

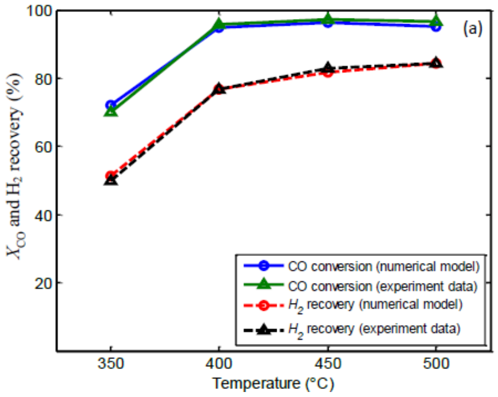

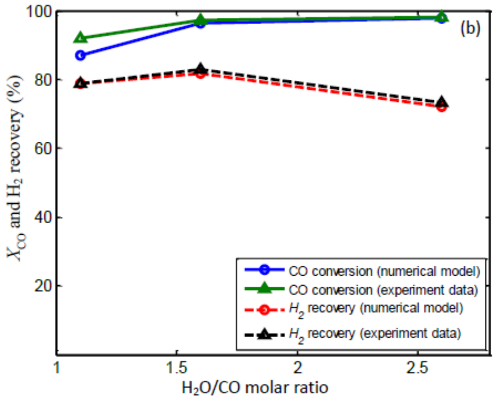

Fig. 2 Comparison of numerical model with experimental data by Augustine et al. (2012) for the CO conversion and the H_2 recovery as functions of (a) temperature, (b) H_2O/CO molar ratio.

RESULTS AND DISCUSSION

The main objective of this paper is to analyze the effects of syngas diffuser flow on the CO conversion and H_2 recovery for a tubular WGS-MR. According to the Sievert' law in Eq. (15), the H_2 permeation flux is proportional to the membrane permeance K_P and K_P can be used to represent the performance of membrane fabrication for a fixed membrane thickness. In this study we use pre-exponential factor, Q_0, as the primary parameter to account for the large variations in membrane permeance as reported by Rothenberger et al. (2004). The inlet radius of reactants $R_{r,in} = 0.005$ m and the outer radius in the permeation side $R_p = 0.02$ m are fixed. The outer radius in reaction side outlet, $R_{r,out}$, is varied from 0.005 m to 0.0195 m to study the effects of diffuser channel design. For the convenience of comparison, the membrane reactor length is a fixed value of L = 0.08 m. The inlet velocities of the syngas and sweeping gas are basically the same as those adopted by Chein et al. (2013). The other fixed parameters and catalyst properties adopted in this work, as shown in Table 1.

Table 1 Parameters and properties used in simulation.

Name	Value	Reference
Catalyst density, ρ_{cat}	2476 kg/m^3	Adams and Barton
Catalyst diameter, d_{cat}	2 mm	Marin et al.
Catalyst porosity, ε	0.4	Marin et al.
Catalyst thermal conductivity, λ_{cat}	0.3 W/m/K	Chiappetta et al.
Catalyst tortuosity, τ	5	Adams and Barton
Convection coefficient on membrane, h_m	2.4 W/m^2/K	Madia et al.
Membrane activation energy, E_m	8230 J/mol	Marin et al.
Membrane thickness, δ	70 μm	Chiappetta et al.
Permeation side inlet temperature, T_p	723.15 K	Chein et al.
Permeation side operating pressure, p_p	1 atm	Chiappetta et al.
Reaction side inlet radius, $R_{r,in}$	0.005 m	Chiappetta et al.
Reaction side inlet temperature, T_r	723.15 K	Chein et al.
Reaction side operating pressure, p_r	15 atm	Chein et al.
H_2O/CO molar ratio, ϕ	1	Chiappetta et al.
Reaction side CO molar flow rate, $\dot{n}_{CO,in}$	1.95×10^{-5} mol/s	Chiappetta et al.
Permeation side N_2 molar flow rate, $\dot{n}_{N_2,in}$	9.75×10^{-4} mol/s	

The variations of CO conversion and H_2 recovery with $R_{r,out}$ for the diffuser flow channels are shown in Figs. 3 and 4 respectively. The magnitude of the pre-exponent factor $Q_{0,b}$ is 1×10^{-9} mol m^{-1} s^{-1} Pa$^{-0.5}$ adopted here as a base reference. This value is in the range of Q_0 used by Chein et al. (2013). The results at $R_{r,out} = 0.005$ m in Figs. 3 and 4 are for the cases of straight flow channel where the inlet and outlet radii of the permeation side are the same. As compared with the data for straight flow channel, the results reveal that both the CO conversion (X_{CO}) and H_2 recovery for a WGS-MR are improved by the design of diffuser flow in the reaction channel. In addition, both the X_{CO} and H_2 recovery increase with $R_{r,out}$ for the diffuser flow channels. The improvement of X_{CO} for the diffuser flow channel at larger $R_{r,out}$ is mainly caused by the increasing of syngas residence time in the reaction side, this will lead a longer time for WGS reaction and H_2 permeation through membrane. The amount of H_2 leaving the reaction side through the membrane with larger $R_{r,out}$ is higher than that for the straight flow channel. This fact implies that the WGS reaction is enhanced for the larger Q_0 and $R_{r,out}$ and a higher X_{CO} is achieved according to Le Chatelier's principle.

The horizontal dash line with X_C of 73.1% in Fig. 3 represents the WGS reaction at the equilibrium state. It is known that for the WGS-MR the X_{CO} can be higher than that at the equilibrium state from Dolan et al. (2010). This is due to the fact that the WGS reaction rate r_{wgs} (the reduction rate of CO), as indicated by Eq. (10), is enhanced when H_2 is removed continuously through membrane from the reaction side and then H_2 concentration is reduced. The variation of H_2 recovery with $R_{r,out}$ is shown in Fig. 4. The H_2 recovery also rises with the increasing of $R_{r,out}$. For the straight channel, the H_2 recovery for $Q_0 = Q_{0,b}$ is only 36.3%, but for the diffuser flow design it increases to 70.7% at $R_{r,out} = 0.0195$ m, which is 1.95 times that of the straight channel case. It is also seen that the H_2 recovery increases from 57.9% to 91.1% when $R_{r,out}$ increases from 0.005 m to 0.0195 m for $Q_0 = 2Q_{0,b}$. From the above results they indicate that the diffuser flow design can significantly improve the CO conversion and H_2 recovery performances of a tubular WGS-MR.

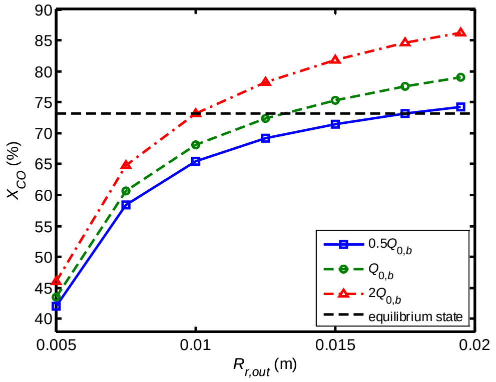

Fig. 3 The CO conversion as a function of $R_{r,out}$ and pre-exponential factor for the diffuser flow channel with L = 0.08 m, where $Q_{0,b} = 1 \times 10^{-9}$ mol m^{-1} s^{-1} Pa$^{-0.5}$.

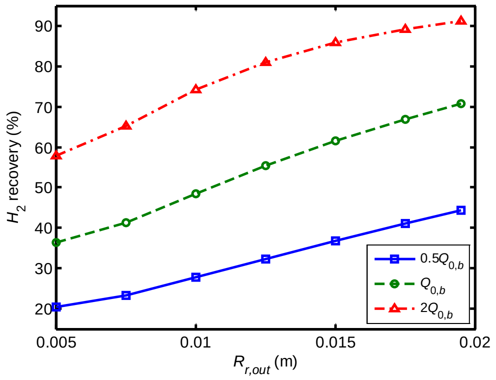

Fig. 4 The H_2 recovery as a function of $R_{r,out}$ and pre-exponential factor for the diffuser flow channel with L = 0.08 m.

For a more clear conception concerned with how the diffuser flow channel works on WGS-MR, the distributions of CO molar fraction, x_{CO}, and H_2 molar fraction, x_{H2}, in the reaction side for $R_{r,out} = 0.005\,m$, $0.010\,m$, $0.0015\,m$, and $0.0195\,m$ are plotted in Figs. 5(a)~(d) and Figs. 6(a)~(d), respectively, for $Q_0 = Q_{0.b}$. The pictures in Figs. 5(a)~(d) show that the x_{CO} decreases monotonically as flowing downstream, and it decreases faster for higher values of $R_{r,out}$. Figs. 6(a)~(d) show that the x_{H2} increases monotonically along z for the straight flow channel. But for the diffuser flow channel, the x_{H2} increases downstream in the beginning, and it increases faster for higher values of $R_{r,out}$. Finally the x_{H2} reaches its maximum value at a certain position of centerline inside the channel. The location with maximum x_{H2} is at z = 0.0462 m (near the center of channel) for $R_{r,out}$ = 0.0195 m. This location moves downstream for lower values of $R_{r,out}$.

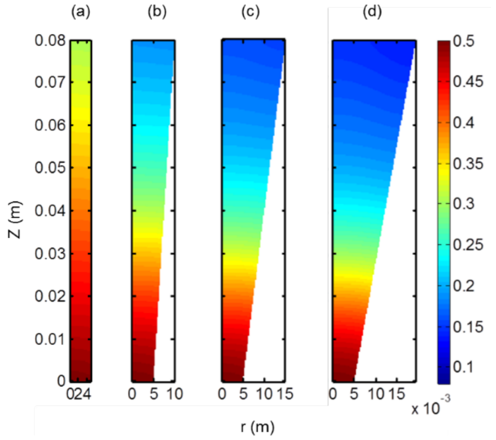

Fig. 5 The distribution of x_{CO} under various $R_{r,out}$ for $Q_0 = 1 \times 10^{-9}$ mol m^{-1} s^{-1} Pa$^{-0.5}$ (a) $R_{r,out} = 0.005$ m, (b) $R_{r,out} = 0.01$ m, (c) $R_{r,out} = 0.015$ m, (d) $R_{r,out} = 0.0195$ m.

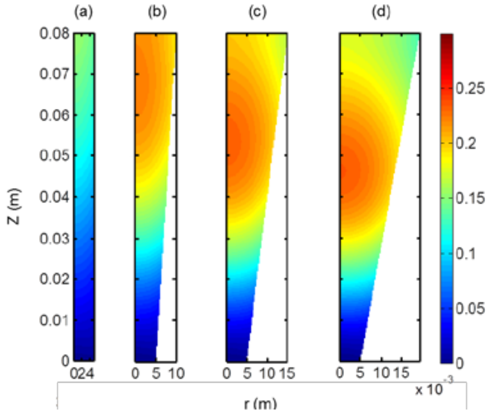

Fig. 6 The distribution of x_{H2} in reaction side under various $R_{r,out}$ for $Q_0 = 1 \times 10^{-9}$ mol m^{-1} s^{-1} Pa$^{-0.5}$ (a) $R_{r,out} = 0.005$ m, (b) $R_{r,out} = 0.01$ m, (c) $R_{r,out} = 0.015$ m, (d) $R_{r,out} = 0.0195$ m.

For the straight flow channel case, Fig. 7 plots the variations of x_{H2} at membrane along the z direction for various Q_0's for L = 0.08 m. The curve of $Q_0 = 0$ represents the limiting case of the membrane without H_2 permeation, that is, the membrane is replaced by a thin solid wall. The curve of $Q_0 = 0$ provides the base information of WGS reaction itself without any reaction enhancement by H_2 permeation through membrane. Fig. 7 shows that the x_{H2} at exit for $Q_0 = 0$ is still far away from the equilibrium state. For the curve of $Q_0 \neq 0$, it is seen that the x_{H2} also increases quickly with z in the beginning, and the increasing speed is smaller for higher Q_0. This is due to the fact that since the inlet syngas is only composed by CO and H_2O, the WGS reaction rate is fast initially and H_2 permeation is relatively small due to low H_2 molar fraction. In other words, the production rate of H_2 is fast in the beginning, since the reaction is still far away from the equilibrium state, the H_2 molar fraction is mainly controlled by the WGS reaction in the entrance region. The x_{H2} increases as the gas keeps flowing downstream where the reaction rate gradually slows down. Meanwhile the H_2 permeation starts to greatly influence the x_{H2} for higher Q_0, the influence of H_2 permeation gradually catches up with that of WGS reaction such that the profile of x_{H2} becomes more flattened at exit for $Q_0 = 2Q_{0,b}$.

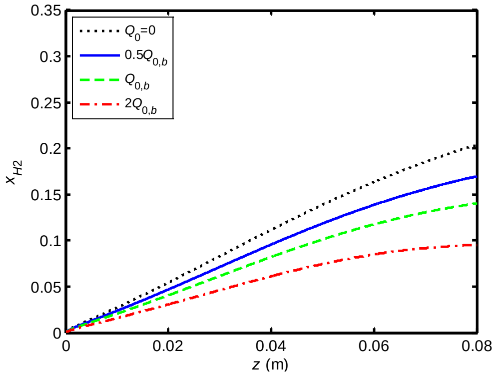

Fig. 7 The molar fraction of H_2 at membrane as a function of z under various Q_0 for the straight flow channel with L = 0.08 m.

The variation of x_{H2} at membrane with z for the diffuser flow channel in the extreme case of $R_{r,out} = 0.0195$ m is plotted in Fig. 8 for L = 0.08 m. The value of x_{H2} approaches to a constant value of about 0.35 for $Q_0 = 0$ at the exit. As compared with the result in Fig. 7, it indicates that a significant enhancement on the WGS reaction rate is found for the design of diffuser flow channel due to a great increase in the residence time for syngas flowing through the reaction channel.

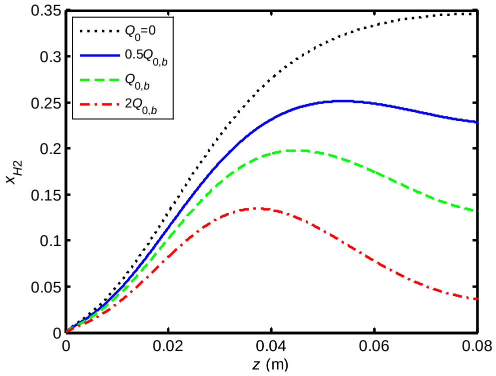

Fig. 8 The molar fraction of H_2 at membrane as a function of z under various Q_0 for the diffuser flow channel with $R_{r,out} = 0.0195$ m and L = 0.08 m.

The curves of $Q_0 \neq 0$ in Fig. 8 show very different behaviors from those for the straight flow channel in Fig. 7. There is a maximum value for each curve with $Q_0 \neq 0$. For example, the maximum value occurs at $z_{max} = 0.045$ m, which is near the middle of channel for $Q_0 = Q_{0,b}$. The locations of maximum values move upstream for higher Q_0. However, this phenomenon does not happen for the straight flow channel case, as shown in Fig. 7. It is also seen that the effect of Q_0 on x_{H2} is significant. For z $< z_{max}$, the x_{H2} climbing is mainly due to the H_2 production by WGS reaction. All the curves are close in the entrance region in Fig. 8, which reveals that the H_2 permeation through membrane is very weak due to very low H_2 concentration in inlet region. For $z > z_{max}$, the x_{H2} decline is mainly due to the H_2 permeation through membrane, and the effect from H_2 permeation increases with z. Since the curve of $Q_0 = 0$ shows that the WGS reaction without any reaction enhancement by H_2 permeation, and there is a very large deviation of x_{H2} between $Q_0 = 0$ and higher value of Q_0 in the exit region. This indicates that the reduction of x_{H2} is mainly controlled by the H_2 through permeation for higher Q_0 in the exit region.

To examine the effects of $R_{r,out}$ on x_{H2}, the x_{H2} at the membrane along the z direction for $R_{r,out}$= 0.01 m, and 0.015 m are shown in Figs. 9(a) and 9(b), respectively. It is seen that the maximum points of x_{H2} curves exist for $Q_0 \neq 0$ when the values of Q_0 and $R_{r,out}$ are large. The location of z_{max} depends on both Q_0 and $R_{r,out}$. Higher value of Q_0 and $R_{r,out}$ makes the value of z_{max} become smaller.

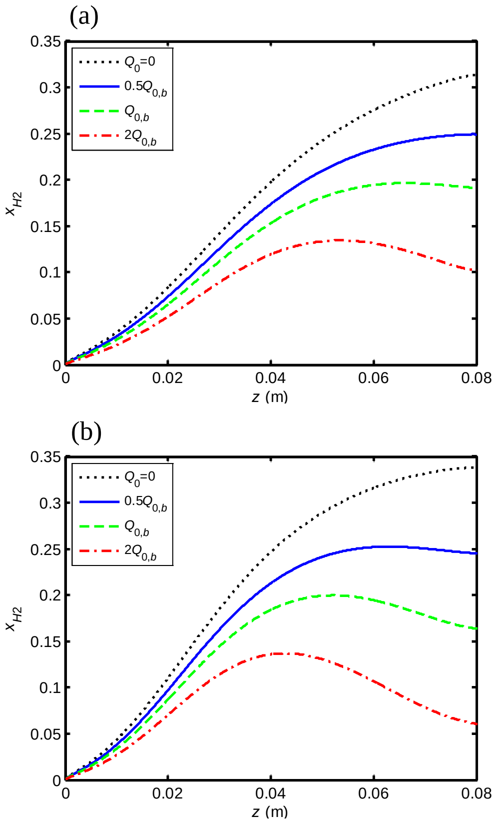

Fig. 9 The molar fraction of H_2 at membrane as a function of z under various Q_0 for the diffuser flow channel with L = 0.08 m for (a) $R_{r,out} = 0.01$ m, (b) $R_{r,out} = 0.015$ m.

The variations of CO molar fractions, x_{CO}'s, at the membrane along the z direction for the straight flow channel and the diffuser flow channel with $R_{r,out}$ = 0.0195 m are plotted in Figs. 10, and 11, respectively. For the straight flow channel, the results in Fig. 10 show that the x_{CO} decreases slowly with increasing of *z*, and the effect of Q_0 on x_{CO} is small. But for the diffuser flow channel, the x_{CO} in Fig. 11 decreases very fast for *z* < 0.05 m because of longer residence time provided for WGS reaction. The x_{CO}'s at exit for the diffuser flow channel is much smaller than those for the straight flow channel. This points out that the WGS reaction is significantly enhanced for the diffuser flow channel with larger $R_{r,out}$.

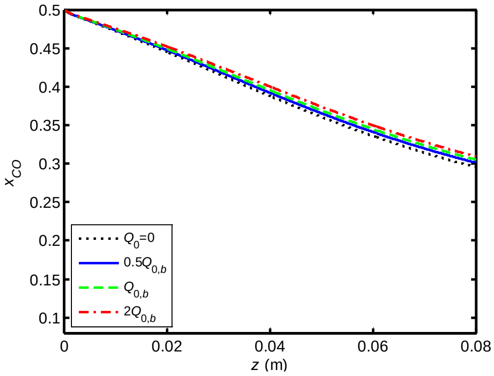

Fig. 10 The molar fraction of CO at membrane as a function of *z* under various Q_0 for the straight flow channel with *L* = 0.08 m.

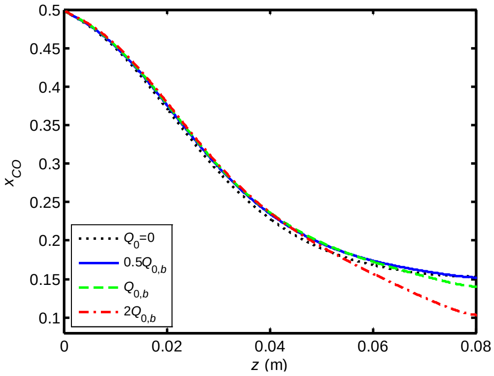

Fig. 11 The molar fraction of CO at membrane as a function of *z* under various Q_0 for the diffuser flow channel with $R_{r,out} = 0.0195$ m and *L* = 0.08 m.

It is seen in Fig. 11 that the effect of Q_0 on x_{CO} is small in the region for *z* < 0.055 m. However, the curve with higher Q_0 begins to separate from that of $Q_0 = 0$ for *z* > 0.06 m. It is seen that the deviation of x_{CO} between $Q_0 = 0$ and $2Q_{0,\mathrm{b}}$ becomes large at exit. Since the curve of $Q_0 = 0$ represents the WGS reaction without enhancement by H_2 permeation, it becomes flattened in the exit region which shows that the WGS reaction is very small. A large deviation of x_{CO} between $Q_0 = 0$ and $2Q_{0,\mathrm{b}}$ in exit region indicates that the reaction enhanced by H_2 permeation through membrane is a driving mechanism to reduce x_{CO}. This provides an additional evidence to interpret that the WGS reaction rate is mainly controlled by the reaction enhancement of H_2 permeation in region near exit for higher values of Q_0 and $R_{r,out}$.

CONCLUSIONS

A 2D model on the performance of a tubular WGS-MR with a new channel design of diffuser flow is investigated. The pre-exponential factor, Q_0, and outer radius at reaction side outlet, $R_{r,out}$, are used as the parameters to account for the membrane permeance variation and the expansion degree of diffuser flow channel, respectively. Based on our numerical results with the parameters adopted in this work, the conclusions are as follows.

(1) Both the CO conversion (X_{CO}) and H_2 recovery for a WGS-MR are improved by the design of diffuser flow channel as a reaction space.
(2) The H_2 molar fraction (x_{H2}) increases monotonously along z (streamwise direction) for the straight flow channel. But for the diffuser flow, there exists a maximum value of x_{H2} at a location inside the channel, and this location moves upstream for higher value of Q_0 and $R_{r,out}$.
(3) The WGS reaction is significantly enhanced for the diffuser flow channel with larger $R_{r,out}$ and Q_0, thus a CO conversion greater than the equilibrium value can be achieved at a much shorter channel length than that for the straight flow channel.
(4) For the diffuser flow channel with higher Q_0 and $R_{r,out}$, the x_{H2} along *z* direction is mainly influenced by the WGS reaction and the H_2 permeation through membrane is weak in the inlet region. However, the reduction of x_{H2} is mainly controlled by the H_2 permeation and the reaction enhanced by H_2 permeation is a driving mechanism to reduce x_{CO} in the exit region.

REFERENCES

Adams, T.A. and Barton, P.I., "A dynamic two-dimensional heterogeneous model for water gas shift reactors," Int. J. Hydrogen Energy Vol. 34, pp. 8877-91(2009).

Augustine, A.S., Ma, Y.H. and Kazantzis, N.K., "High pressure palladium membrane reactor for the high temperature water-gas shift reaction," Int. J. Hydrogen Energy 36, pp. 5350-5360(2011).

Augustine, A.S., Mardilovich, I.P., Kazantzis, N.K. and Ma, Y.H., "Durability of PSS-supported Pd-membranes under mixed gas and water-gas shift conditions," J. Membr. Sci. 415-416, pp. 213-220(2012).

Barbieri, G., Brunetti, A., Tricoli, G. and Drioli, E., "An innovative configuration of a Pd-based membrane reactor for the production of pure hydrogen- Experimental analysis of water gas shift," J. Power Sources 182, pp. 160-167(2008).

Basile, A., Criscuoli, A., Santella, F. and Drioli, E., "Membrane reactor for water-gas shift reaction," Gas Sep. Purif. 10, pp. 243-54(1996).

Boon, J., Li, H., Dijkstra, J.W. and Pieterse, J.A.Z., "2-Dimensional membrane separator modelling: mass transfer by convection and diffusion," Energy Procedia 4, pp. 699-706(2011).

Brunetti, A., Caravella, A., Barbieri, G. and Drioli, E., "Simulation study of water-gas shift reaction in membrane reactor," J. Membr. Sci. 306, pp. 329-340(2007).

Chein, R.Y., Chen, Y.C. and Chung, J.N., "A parametric study of membrane reactors for hydrogen production via high-temperature water gas shift reaction," Int. J. Hydrogen Energy 38, pp. 2292-2305(2013).

Chen, W.H. and Chein, R., "Hydrogen production from coal-derived syngas undergoing high-temperature water gas shift reaction in a membrane reactor," Int. J. Energy Research 42, pp. 2940-2952(2018).

Chen, W.H. and Lu, J.J., "Hydrogen production from water gas shift reactions in association with separation using a palladium membrane tube," Int. J. Energy Research 36, pp. 346-354(2012).

Chen, W.H., Syu, W.Z. and Hung, C.I., "Numerical characterizationon concentration polarization of hydrogen permeation in a Pd-based membrane tube," Int. J. Hydrogen Energy 36, pp. 14734-14744(2012).

Chen, W.H., Syu, W.Z., Hung, C.I., Lin, Y.L. and Yang, C.C., "Influences of geometry and flow pattern on hydrogen separation in a Pd-based membrane tube," Int. J. Hydrogen Energy 38, pp. 1145-1156(2013).

Chen, W.H., Tsai C.W., Lin Y.L., Chein R.Y. and Yu C.T.,"Reaction phenomena of high-temperature water gas shift reaction in a membrane reactor," Fuel 199, pp. 358-371(2017).

Chiappetta, G., Clarizia, G. and Drioli, E., "Theoretical analysis of the effect of catalyst mass distribution and operation parameters on the performance of a Pd-based membrane reactor for water-gas shift reaction," Chem. Eng. J. 136, pp. 373-382(2008).

Cornaglia, C.A., Tosti, S., Sansovini, M. and Munera, J., "Novel catalyst for the WGS reaction in a Pd-membrane reactor," Appl. Catal. A: Gen. 462- 463, pp. 278- 286(2013).

Coroneo, M., Montante, G., Catalano, J. and Paglianti, A., "Modelling the effect of operating conditions on hydrodynamics and mass transfer in a Pd-Ag membrane module for Hydrogen purification," J. Membr. Sci. 343, pp. 34-41(2009).

Diniz da Costa, J. C., Reed, G.P. and Thambimuthu, K., "High temperature gas separation membranes in coal gasification," Energy Procedia, 1, pp. 295-302(2009).

Dolan, M.D., Donelson, R. and Dave, N.C., "Performance and economics of a Pd-based planar WGS membrane reactor for coal gasification," Int. J. Hydrogen Energy 35, pp. 10994-11003(2010).

Galuszka, J., Giddings, T. and Iaquaniello, G., "Membrane assisted WGSR- Experimental study and reactor modeling," Chem. Eng. J. 213, pp. 363-370(2012).

Gosiewski, K. and Tanczyk, M., "Applicability of membrane reactor for WGS coal derived gas processing: Simulation-based analysis," Catal. Today 176, pp. 373- 382(2011).

Iyoha, O., Enick, R., Killmeyer, R., Howard, B., Ciocco, M. and Morreale, B., "Hydrogen production from simulated coal syngas containing H2S inmulti-tubular Pd and 80 wt% Pd-20 wt% Cu membranereactors at 1173 K," J. Membr. Sci. 306, pp. 103-115(2007).

Madia, G.S., Barbieri, G. and Drioli, E., "Theoretical and experimental analysis of methane steam reforming in a membrane reactor," Can. J. Chem. Eng. 77, pp. 698-706(1999).

Marin, P., Diez, F.V. and Ordonez, S., "Fixed bed membrane reactorsfor WGSR-based Hydrogen production: optimisation of modelling approaches and reactor performance," Int. J. Hydrogen Energy 37, pp. 4997-5010(2012).

Merkel, T.C., Zhou, M. and Baker, R.W., "Carbon dioxide capture with membranes at an IGCC power plant," J. Membr. Sci. 389, pp. 441-450(2012).

Mills, A.F., Mass transfer, Englewood Cliffs, New Jersey: PenticeHall(2001).

Moe, J.M., "Design of water gas shift reactors," Chem. Eng. Prog. 58, pp. 33-36(1962).

Nield, D.A. and Bejan, A., Convection in Porous Media, Springer-Verlag, 3rd edition, New York (2006).

Piemonte, V., Falco, M.D., Favetta, B. and Basile, A., "Counter-current membrane reactor for WGS process: Membrane design," Int. J. Hydrogen Energy 35, pp. 12609-12617(2010).

Rothenberger, K.S., Cugini, A.V., Howard, B.H., Killmeyer, R.P., Ciocco, M.V., Morreale, B.D., Enick, R.M., Bustamante, F., Mardilovich, I.P. and Ma, Y.H., "High pressure hydrogen permeance of porous stainless steel coated with a thin palladium film via electroless plating," J. Membr. Sci. 244, pp. 55-68(2004).

Schiebahn, S., Riensche, E., Weber, M. and Stolten, D., "Integration of H2-selective membrane reactors in the integrated gasification combined cycle for CO2 separation," Chem. Eng. Technol. 35, pp. 555–560(2012).

Vadlamudi, V.K. and Palanki, S., "Modeling and analysis of miniaturized methanol reformer for fuel cell powered mobile applications," Int. J. Hydrogen Energy 36, pp. 3364-3370(2011).

Ward, L. and Dao, T., "Model of Hydrogen permeation behavior in palladium membranes," J. Membr. Sci. 153, pp. 211-231(1999).

NOMENCLATURE

c_p	Specific heat, J kg^{-1} K^{-1}
C_f	Forchheimer drag coefficient
d_{cat}	Catalyst particle diameter of, m
D	Mass diffusion coefficient, m^2 s^{-1}
E_m	Active energy of membrane, J mol^{-1}
h_m	Heat transfer coefficient at the membrane, W m^{-2} K^{-1}
$\vec{I}$	Unit tensor
J_{H_2}	H_2 flux, mol m^{-2} s^{-1}
K	Catalyst bed permeability, m^{-2}
K_{eq}	Equilibrium constant
K_p	Membrane permeance
L	Membrane length
m	Mass fraction
M	Molecular weight, kg mol^{-1}
$\dot{n}$	Molar flow rate, mol s^{-1}
p	Pressure, Pa
q_c	Chemical reaction heat source term in energy equation, W m^{-3}
Q_0	Pre-exponential factor, mol m^{-1} s^{-1} Pa$^{-0.5}$
r	Reaction rate, kg m^{-3} s^{-1}
r_{wgs}	Water-gas shift reaction rate, mol m^{-3} s^{-1}
R	Radius, m
Re	Reynolds number
R_g	Gas constant, J K^{-1} mol^{-1}
S_u	Source term in momentum equation, N m^{-2}
T	Temperature, K
$\bar{v}$	Averaged inlet velocity, m s^{-1}
$\vec{V}$	Velocity vector, m s^{-1}
x	Molar fraction
X_{CO}	CO conversion
z_{max}	Location of maximum H_2 molar fraction, m

Greek Symbols

ΔH_{wgs}	Heat of water-gas shift reaction, J mol^{-1}
δ	Membrane thickness, m
ε	Reaction side porosity
λ	Thermal conductivity coefficient, W m^{-1} K^{-1}
μ	Viscosity, kg m^{-1} s^{-1}
ϕ	H_2O/CO molar ratio
ρ	Density, kg m^{-3}
τ	Tortuosity

Subscripts

b	Base reference
cat	Catalyst
e	Effective
g	Gas mixture
i	Species of i
in	Inlet
m	Membrane
out	Outlet
p	Permeation side
r	Reaction side
⊥	Normal direction

擴張流對水氣轉移膜反應器性能之效應

林昱劭 許文震
國立清華大學動力機械工程學系

陳炎洲
國立聯合大學能源工程學系

摘要

以鈀為基底的水氣轉移膜反應器(WGS-MR)是一項具有發展性的技術，可用在燃燒前的CO_2捕捉與產氫反應上。本文以數值模擬的方式分析合成氣在漸擴管中內部的流場對於WGS-MR效能的影響。結果顯示WGS-MR的CO轉換率與H_2的回收都有所提升。從物理學的觀點，將管狀的WGS-MR改成漸擴結構，將能增加H_2通過膜的時間與WGS的反應時間，以達到提升效能的目的。